



Clinical neuroanatomy

Organising white matter in a brain without corpus callosum fibres

Audrey Bénézit^{a,b,c}, Lucie Hertz-Pannier^{d,e,f},
 Ghislaine Dehaene-Lambertz^{a,b,c}, Karla Monzalvo^{a,b,c},
 David Germanaud^{d,e,f}, Delphine Duclap^{g,c}, Pamela Guevara^{g,c},
 Jean-François Mangin^{g,c}, Cyril Poupon^{h,c}, Marie-Laure Moutardⁱ and
 Jessica Dubois^{a,b,c,*}

^a INSERM, U992, Cognitive Neuroimaging Unit, France

^b CEA, UNICOG, NeuroSpin, Gif-sur-Yvette, France

^c University Paris Sud, Orsay, France

^d CEA, UNIACT, NeuroSpin, Gif-sur-Yvette, France

^e INSERM, U663, Paris, France

^f University Paris Descartes, Paris, France

^g CEA, UNATI, NeuroSpin, Gif-sur-Yvette, France

^h CEA, UNIRS, NeuroSpin, Gif-sur-Yvette, France

ⁱ Trousseau Hospital, Neuropediatrics Department, Paris, France

ARTICLE INFO

Article history:

Received 7 January 2014

Reviewed 20 February 2014

Revised 29 June 2014

Accepted 25 August 2014

Action editor Marco Catani

Published online 11 September 2014

Keywords:

Corpus callosum dysgenesis

agenesis

Hypoplasia

MRI

ABSTRACT

Isolated corpus callosum dysgenesis (CCD) is a congenital malformation which occurs during early development of the brain. In this study, we aimed to identify and describe its consequences beyond the lack of callosal fibres, on the morphology, microstructure and asymmetries of the main white matter bundles with diffusion imaging and fibre tractography. Seven children aged between 9 and 13 years old and seven age- and gender-matched control children were studied. First, we focused on bundles within the mesial region of the cerebral hemispheres: the corpus callosum, Probst bundles and cingulum which were selected using a conventional region-based approach. We demonstrated that the Probst bundles have a wider connectivity than the previously described rostrocaudal direction, and a microstructure rather distinct from the cingulum but relatively close to callosal remnant fibres. A sigmoid bundle was found in two partial agenesises. Second, the corticospinal tract, thalamic radiations and association bundles were extracted automatically via an atlas of adult white matter bundles to overcome bias resulting from a priori knowledge of the bundles' anatomical

Abbreviations: AF, arcuate fasciculus (postAF, posterior segment); CC, corpus callosum; CCD, corpus callosum dysgenesis; CCag, corpus callosum agenesis; CG, cingulum (infCG / supCG, inferior / superior segments); CSF, cerebro-spinal fluid; CST, corticospinal tract; <D>, mean diffusivity; DTI, diffusion tensor imaging; DWI, diffusion-weighted imaging; FA, fractional anisotropy; iFOF, inferior fronto-occipital fasciculus; HARDI, high angular resolution diffusion imaging; ILF, inferior longitudinal fasciculus; MRI, magnetic resonance imaging; OR, optic radiations; PB, Probst bundles; PR, thalamic radiations projecting to the parietal lobe; RGB, colour-coded directionality map; SLF, superior longitudinal fasciculus; UF, uncinate fasciculus.

* Corresponding author. CEA/SAC/DSV/I2BM/NeuroSpin/Cognitive Neuroimaging Unit U992, Bât 145, point courrier 156, 91191 Gif-sur-Yvette, France.

E-mail address: jessica.dubois@centraliens.net (J. Dubois).

<http://dx.doi.org/10.1016/j.cortex.2014.08.022>

0010-9452/© 2014 Published by Elsevier Ltd.

Diffusion tensor imaging DTI
Tractography
Child
White matter bundles
Probst bundle
Atlas

morphology and trajectory. Despite the lack of callosal fibres and the colpocephaly observed in CCD, all major white matter bundles were identified with a relatively normal morphology, and preserved microstructure (i.e. fractional anisotropy, mean diffusivity) and asymmetries. Consequently the bundles' organisation seems well conserved in brains with CCD. These results await further investigations with functional imaging before apprehending the cognition variability in children with isolated dysgenesis.

© 2014 Published by Elsevier Ltd.

1. Introduction

The corpus callosum is the largest pool of white matter fibres which connect cerebral regions across hemispheres (Witelson, 1989) and are responsible for the transfer of sensory, motor and cognitive information between homotopic cortical areas. While genetic constraints are fundamental for the hemispheric specialisation of lateralised functions, callosal fibres are also supposed to play a key role (Cook, 1984) in the lateralisation related to hand preference (Beaule, Tremblay, & Theoret, 2012) and left-hemisphere language processing (Bloom & Hynd, 2005); however the excitatory and inhibitory nature of information travelling between the two hemispheres is debated. On the one hand, the theory of inhibition states that the corpus callosum would favour the development of hemispheric lateralisation by providing a pathway through which one hemisphere could inhibit the other to dominate a given function (Cook, 1984; Hellige, 1993). On the other hand, the theory of excitation supports that the corpus callosum would enhance the integration of cerebral processing between the two hemispheres by activating the unstimulated hemisphere (Galaburda, 1984; Lasseonde, 1986). Since functional asymmetries are associated with anatomical asymmetries of sulci depth (Cykowski et al., 2008) and white matter microstructure (Takao, Abe, et al., 2011; Takao, Hayashi, & Ohtomo, 2011), it has been suggested that the development and selective pruning of callosal fibres may be related to these structural asymmetries (Aboitiz, Scheibel, Fisher, & Zaidel, 1992; Aboitiz, Scheibel, & Zaidel, 1992; Cherbuin et al., 2013; Witelson & Nowakowski, 1991).

The development of the corpus callosum starts early on during pregnancy, between 14 and 18 weeks of gestation (Ren et al., 2006), and displays a protracted maturation throughout childhood and adolescence (Lebel, Caverhill-Godkewitsch, & Beaulieu, 2010). Corpus callosum dysgenesis (CCD), either agenesis (CCAg) or hypoplasia, is a congenital malformation. Agensis is defined by complete or partial absence of corpus callosum fibres, and its aetiological spectrum is varied: genetic syndromes (almost 400 described), chromosomal abnormalities, metabolic disorders, infections, teratogens, etc. (Vasudevan, McKechnie, & Levene, 2012). However, aetiology is not always found, particularly when the malformation is isolated. The pathological mechanism responsible for agensis occurs early on, between 14 and 18 weeks of gestation (Ren et al., 2006): fibres from the cortex fail to cross the midline and are deemed to constitute in each cerebral hemisphere an aberrant longitudinal tract named a "Probst bundle" (Probst,

1901), which has been described as running in a rostrocaudal direction, laterally to the superior part of the cingulum bundle. Corpus callosum hypoplasia is clearly distinguishable from agensis since it is defined as a homogeneous reduction of the callosal size. Most homotopic cortical areas of the two hemispheres are connected, implying a preservation of the callosal sub-divisions (rostrum, genu, body and splenium from its anterior to its posterior extremities), but with a restricted number of axons. When the distinction between corpus callosum agensis and hypoplasia is being discussed, detecting Probst bundles in anatomical imaging commonly guides the diagnosis towards corpus callosum agensis.

For about 20 years, the progress of prenatal ultrasound has enabled the systematic screening of corpus callosum abnormalities during the second trimester of pregnancy. Most of the time, the diagnosis of dysgenesis is confirmed by conventional foetal MRI. CCD can be either isolated (in one third of cases), or complex (in two-thirds of cases), when associated with other cerebral or extra-cerebral abnormalities, genetic syndromes, chromosomal anomalies or metabolic diseases (Fratelli et al., 2007). A wide spectrum of neuropsychological disorders has been described in patients with CCD (Chadie et al., 2008; Paul et al., 2007), ranging from severe developmental delay, neurologic symptoms and behavioural deficits to normal development. While outcome is poor in complex cases, it is mostly favourable when dysgenesis is isolated: nearly 75% of children have normal intelligence, but they frequently present mild learning difficulties (Moutard et al., 2012). The prevalence of this malformation is difficult to assess since malformation is not always diagnosed during pregnancy, it can be asymptomatic after birth, and it covers a spectrum of varying severity. According to Paul and collaborators, CCAg occurs in at least 1/4000 live births, and is found in 3–5% of patients with developmental disorders (Paul et al., 2007). In a Californian study, the prevalence of CCD was 1.8/10,000 live births (1.4/10,000 CCAg and .4/10,000 corpus callosum hypoplasia) (Glass, Shaw, Ma, & Sherr, 2008).

Actually, the split-brain organisation in the case of isolated dysgenesis has been scarcely described. Firstly, given their proximity and the involvement of cingulate cortex during early callosal development (Ren et al., 2006), how do fibres from the corpus callosum, the Probst bundles and the cingulum interlink together in the dysgenetic brain? Secondly, how does the lack of callosal fibres unsettle the morphology of projection and association bundles, and how does the colpocephaly, frequently observed in CCD, influence the morphology of posterior bundles? Even though the white

matter intensity is not different on conventional T1- and T2-weighted MR images of CCD patients, the bundles' microstructure may differ from control subjects, and the inter-individual variability in cognitive performances suggests different connectivity patterns from one subject to another. Furthermore, exploring inter-hemispheric asymmetries of white matter bundles in brains with CCD may contribute to better understand the role of callosal fibres in the establishment of functional lateralisation in the developing brain.

A systematic description of the white matter organisation and microstructure is still lacking in dysgenetic brains as it requires a reproducible methodology and quantitative parameters to precisely characterise individual subjects. Nowadays, diffusion-weighted imaging (DWI) and fibre tractography have enabled researchers and physicians to virtually delineate and reconstruct the white matter fibre trajectories in vivo and in three-dimensional spaces, based on the anisotropic nature of water molecule diffusion within axonal bundles (for a review, (Le Bihan & Johansen-Berg, 2012)). The diffusion tensor model further enables the quantification of diffusion parameters (e.g. fractional anisotropy, mean diffusivity), which reflect the tissue microstructure (fibre organisation, compactness, density and maturation) (for reviews, (Beaulieu, 2002; Dubois, Dehaene-Lambertz, et al., 2014a) in regions of interest (ROIs) or tracts (Dubois, Hertz-Pannier, Dehaene-Lambertz, Cointepas, & Le Bihan, 2006).

In corpus callosum agenesis, studies using diffusion tensor imaging (DTI) and tractography based on regions of selection (Catani, Howard, Pajevic, & Jones, 2002; Huang, Zhang, van Zijl, & Mori, 2004) have described the organisation of Probst bundles, as longitudinal tracts connecting frontal and occipito-parietal lobes and blending with anterior callosal remnant fibres in partial agenesis (Lee, Mori, Kim, Kim, & Kim, 2004; Tovar-Moll et al., 2007). Their microstructure seems well organised from early on with relatively high anisotropy values in comparison with other tracts (Lee et al., 2004). In partial CCAg, Wahl and colleagues have highlighted various patterns of callosal remnant connectivity, not exclusively frontal, but also temporo-occipital or fronto-occipital without parietal connections (Wahl et al., 2009). Moreover, in patients with partial agenesis or hypoplasia, an aberrant sigmoid bundle has been inconsistently identified between the frontal lobe and the contralateral parieto-occipital region, through the genual remnant or the hypoplastic body of the corpus callosum (Tovar-Moll et al., 2007). To our knowledge, only one study has shown the relatively normal organisation of other association and limbic white matter bundles (fronto-occipital, arcuate and superior longitudinal fascicles, cingulum) in three subjects with corpus callosum agenesis (Forkel et al., 2014), but the authors did not characterise the bundles' microstructure with DTI parameters nor did they report the degree of asymmetry for these bundles relative to the normal brain.

In this context, the purpose of this study was two-fold. First, we focused on the macro- and microstructure of the "corpus callosum complex" (corpus callosum, Probst bundle and cingulum), whose fibres were selected with a conventional region-based approach. Second, we described the organisation of the main bundles (corticospinal tract, thalamic radiations and association bundles) segmented with an atlas-based approach (Guevara et al., 2012). Differences in

Table 1 – Characteristics of the dysgenesis children. For each child, the following data are presented: description of the corpus callosum dysgenesis, age, gender, Intellectual Quotient (IQ), school courses, presence of the sigmoid bundle on tractography.

	Case1	Case2	Case3	Case4	Case5	Case6	Case7
type of dysgenesis	Complete	Complete	Complete	Partial	Partial	Partial	Hypoplasia
age	13 y5 m	11 y	11 y6 m	10 y8 m	10 y7 m	9 y5 m	10 y2 m
gender	F	F	F	M	F	F	M
IQ	86	94	76	99	97	89	diss. no deficiency
School cursus	Ordinary	Ordinary	Ordinary until 11 y. Specific school	Ordinary	Ordinary	Ordinary	Ordinary
sigmoid bundle	no	no	no	left frontal/right parieto-occipital	no	right frontal/left parieto-occipital	no

Abbreviations: y: years; m: months; F: female; M: male; diss: dissociated.

the pathway trajectories, connectivity patterns, microstructure and asymmetries were evaluated between the dysgenesis and control groups.

2. Materials and methods

2.1. Patients

The study was performed on a population of 12 children who had benefited from the systematic antenatal screening of CCD and from a 10-year medical follow up since their birth (between 1994 and 2000) in Trousseau Hospital (Paris) (Moutard et al., 2012). Note that over an equivalent but more recent time period (between 2000 and 2006), 55 children with isolated CCD were born in the same hospital, among which 33 didn't present neurological anomalies (Isapof et al., 2010).

Among the 12 patients, no child exhibited mental retardation, but 4 children had borderline intelligence ($70 < \text{total IQ} < 79$). The MRI research study was proposed to children with isolated callosum dysgenesis (CCD) (1 child excluded because signs of foetal alcohol syndrome had become obvious) and normal development (all could understand instructions for the MRI protocol, especially not to move during acquisitions). Finally, seven right-handed children with isolated dysgenesis (5 girls; mean age 11 years, range 9 years 5

months – 13 years 5 months) participated in the MRI protocol. Three children presented with a complete CCAg, three a partial CCAg, and one a corpus callosum hypoplasia (see details in Table 1). All had normal psychomotor development, clinical evaluation, and intellectual quotient. Seven healthy controls (with normal cognitive development and normal brain images) were matched by age, sex and handedness (5 girls; mean age 11 years, range 9 years 9 months – 13 years 1 month). Written informed consent was obtained from the children parents. The MRI study protocol was endorsed by the Institution of Paris University Hospitals (“Assistance Publique – Hôpitaux de Paris”) and approved by a regional ethical committee for biomedical research (institutional review board from Kremlin Bicêtre Hospital).

2.2. MR acquisitions

MR imaging was performed on a 3T MRI system (Tim Trio, Siemens Medical Systems, Erlangen, Germany) equipped with a whole body gradient (40 mT/m, 200 T/m/sec) and an 8-channel head coil.

For DWI, a spin-echo single-shot EPI sequence was used, with parallel imaging (GRAPPA reduction factor 2) and partial Fourier sampling (factor 6/8). 40 interleaved axial slices covering the whole brain were imaged with a $1.9 \times 1.9 \times 3 \text{ mm}^3$ spatial resolution (field of

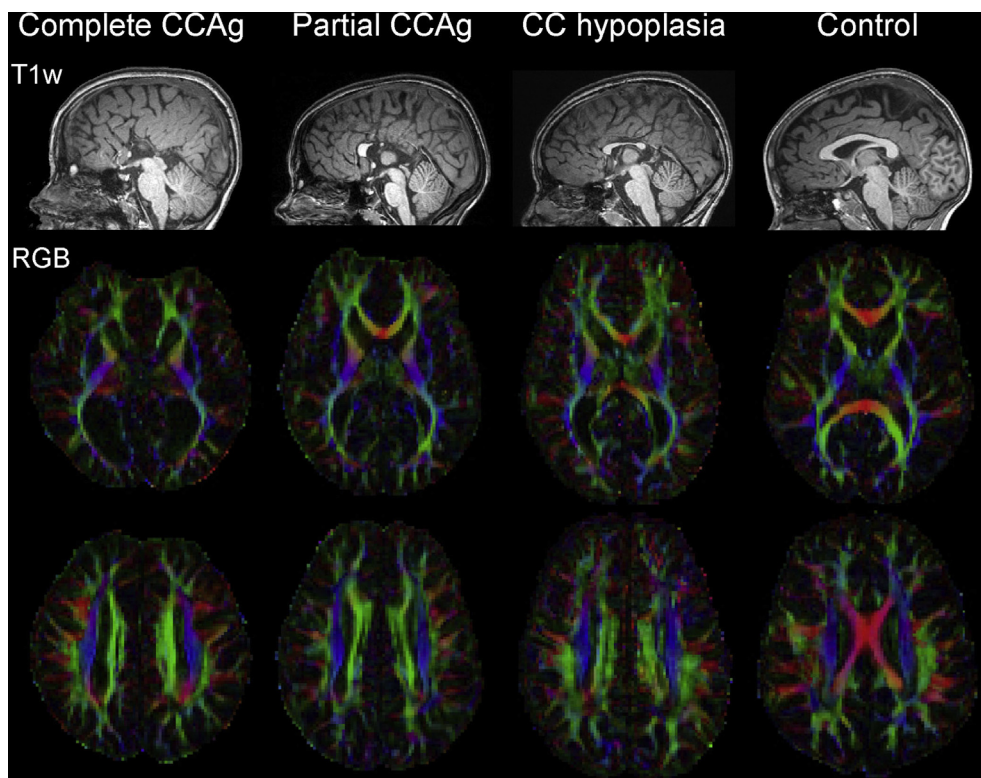


Fig. 1 – T1w images and DTI-RGB maps in typical children. Four examples of children are considered: complete and partial agenesis of the corpus callosum, hypoplasia and a control child. T1w images are presented on a sagittal view at the level of the inter-hemispheric plane. For the child with hypoplasia, note the homothetic reduction of the corpus callosum, with the preserved subdivisions into genu, body and splenium (the rostrum is barely visible). DTI-RGB maps are presented on axial views, at the level of the internal capsule and of the Probst bundle or corpus callosum body (for the control child). On these maps, the colours code for the main diffusion direction which reflects the white matter bundles orientation: red = left-right, green = anterior-posterior, blue = inferior-superior.

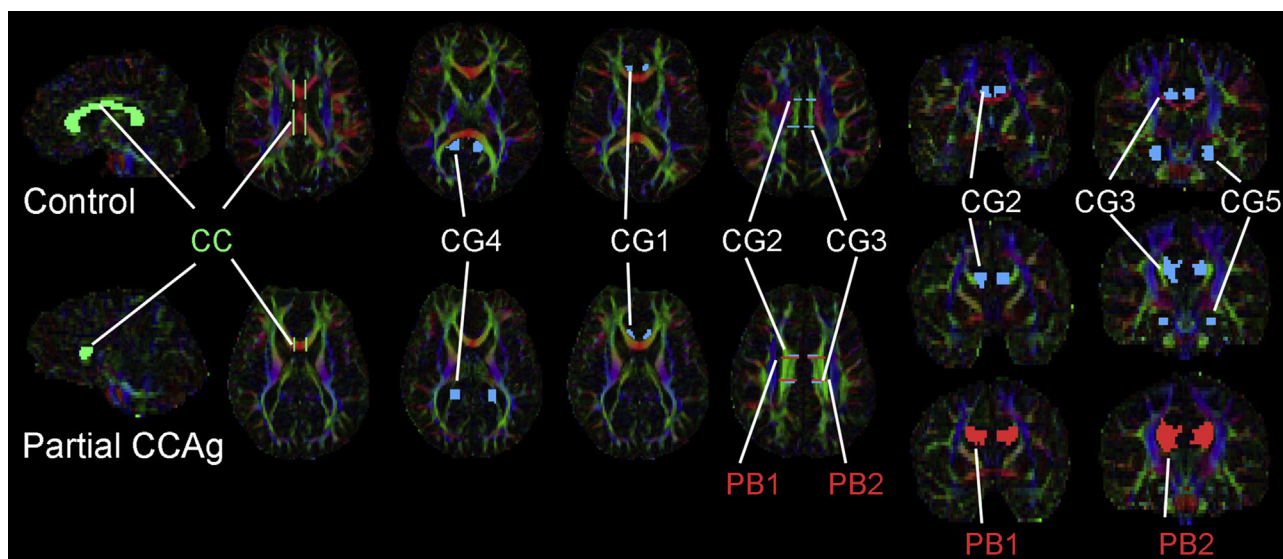


Fig. 2 – Selection of the tracts for the “corpus callosum complex”. ROIs used to select the corpus callosum (CC), cingulum (CG) and Probst bundles (PB) are presented for a control subject (first row) and a patient with partial corpus callosum agenesis (second row).

view = $24 \times 24 \text{ cm}^2$, matrix = 128×128 , slice thickness = 3 mm). After the acquisition of the $b = 0$ volume, diffusion gradients were applied along 30 orientations with $b = 1000 \text{ sec mm}^{-2}$, leading to a total acquisition time of 5 min23 sec (TE = 86 msec, TR = 9.5 sec).

T1-weighted (T1w) anatomical images were acquired with a 3D MP-RAGE inversion sequence with parallel imaging (GRAPPA reduction factor 2). Slices covering the whole brain were imaged with a 1 mm isotropic spatial resolution (TE = 4.18 msec, TI = 900 msec, TR = 2300 msec, acquisition time of 4 min44 sec).

2.3. DWI data post-processing and tractography

Data were visualised with Anatomist software (Riviere et al., 2000) (<http://brainvisa.info/>) and analysed using the PTK toolkit and the Connectomist software developed in-house at NeuroSpin (Duclap et al., 2012). DW images were corrected for motion artefacts and distortions stemming from eddy currents, using a dedicated strategy recently implemented in the lab (Dubois, Kulikova et al., 2014b). During this procedure, DW images were resampled to provide co-registration with T1w anatomical images and to align the anterior and posterior commissures in a single axial slice (AC-PC position). To do so, commissures were identified manually on anatomical images, and $b = 0$ images were co-registered automatically to anatomical images in the AC-PC position. Afterwards, the resulting rigid transformation was applied to all DW images at the same time as the affine transformation to correct for 3D misregistration due to motion and for eddy-current distortions (Dubois, Kulikova et al., 2014b).

DTI maps were generated (fractional anisotropy FA, mean $\langle D \rangle$, longitudinal λ_{\parallel} and transverse λ_{\perp} diffusivities, colour-encoded directionality RGB, Fig. 1). Whole brain 3D fibre tractography was based on an analytical Q-ball model (Descoteaux, Angelino, Fitzgibbons, & Deriche, 2007) at order

4, to take into account the relatively low b-value and radial resolution, and on a regularisation using a Laplace-Beltrami operator. To better deal with crossing-fibres, a tractography algorithm based on regularised particle trajectories (Perrin et al., 2005) was used with an aperture angle of 45° and initialisation with 25 seeds per voxel from a mask within the white matter excluding voxels with low FA ($<.2$) or high $\langle D \rangle$ ($>2.10^{-3} \text{ mm}^2 \text{ s}^{-1}$), which may correspond to grey matter or cerebro-spinal fluid (CSF). A few voxels with FA values between .15 and .2 were added manually on the inferior cingulum branching in the temporal lobe because their proximity with CSF caused incorrect exclusion in the initial mask. The resulting seed mask had an average volume of $615 \text{ mL} \pm 66 \text{ mL}$ over the 14 subjects, with no difference between the patient and control groups ([min, max] = [528 mL, 734 mL] corresponding to around 50,000 and 70,000 voxels).

2.4. Selection of white matter bundles

To overcome a priori anatomical knowledge of bundle trajectory and to homogenise their selection across the two groups of children (CCD and controls), the major bundles (except the “corpus callosum complex”, detailed below) were automatically selected through an approach based on intra-subject clustering (Guevara et al., 2011) and on comparison with a multi-subject bundle atlas defined from a group of healthy adults (Guevara et al., 2012). The bundles were identified in each individual dataset according to their morphology, shape and length using a simple affine registration and a criteria of distance between the atlas bundles and the target fibres (Guevara et al., 2012). We considered in the current study:

- Projection bundles: corticospinal tract, optic radiations and thalamic radiations to the parietal lobe (called parietal radiations in the following)

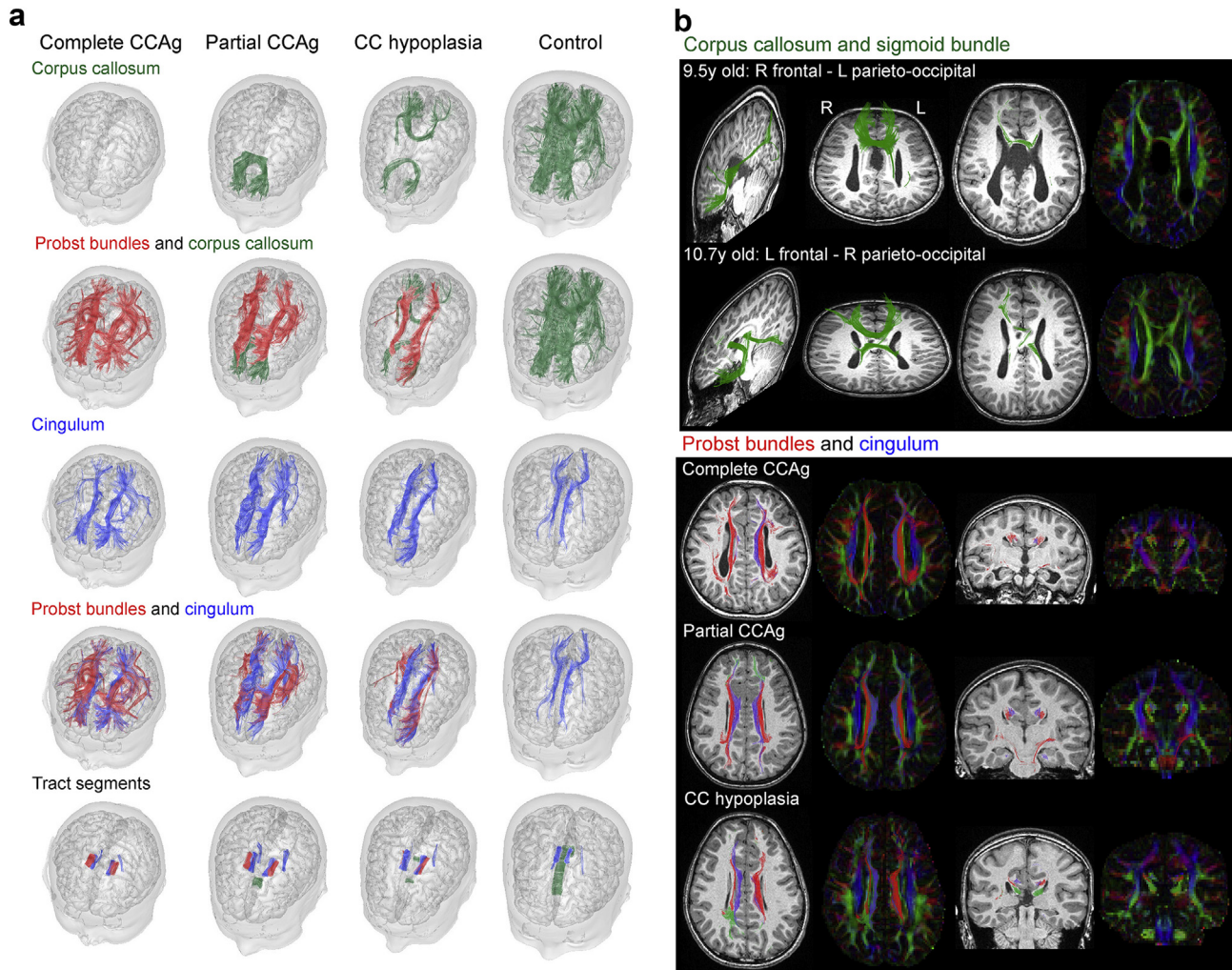


Fig. 3 – Tractography of the “corpus callosum complex”. 3a: The 3D reconstructions of the corpus callosum, Probst bundle and cingulum are presented for the same children as in Fig. 1. The last row outlines the tract segments used for the quantification of DTI parameters (see section II.5 for details): these segments were extracted between the selection regions (Fig. 2) and limited the corpus callosum around the inter-hemispheric fissure, the Probst bundle to a superior segment, and the cingulum to two superior and inferior segments. **3b:** Reconstructions of the corpus callosum and sigmoid tracts are outlined for two children with partial CCAg in the two first rows. 2D views of the Probst bundles and cingulum fibres are shown for the 3 children from Fig. 1 and 3a (with complete, partial CCAg, and hypoplasia) in the two last rows. Images are projected either on anatomical images or on RGB maps.

- Association bundles: arcuate fasciculus (long and posterior segments) (Catani, Jones, & ffytche, 2005), superior and inferior longitudinal fascicles, inferior fronto-occipital fasciculus and uncinate fasciculus.

For all children, the bundle trajectory was visually checked and compared with individual tracts reconstructed according to a region-based approach (visual comparison not shown).

Besides the corpus callosum, the Probst bundles and the cingulum were selected using a conventional region-based approach because the atlas-based approach was inadequate in dysgenic brains for two reasons: 1) the trajectory of remnant callosal fibres in partial CCAg or hypoplasia was too different from healthy callosal fibres; 2) the split between the Probst and cingulum fibres was impossible due to both their

close trajectory and the absence of Probst bundle specification in the atlas. Regions of selection were drawn manually according to anatomical landmarks present in both the control and CCD children; regions were placed as follows, perpendicularly to the bundles' pathways on the overlaid T1w images and DTI-RGB maps (Fig. 2).

For the corpus callosum, two sagittal regions were drawn on either side of the inter-hemispheric plane (with a 9.5 mm distance in-between, corresponding to 5 voxels). For the cingulum bundle, five regions were drawn from anterior to posterior: on the anterior bending (1), on the superior portion of the bundle at the level of the anterior (2) and posterior (3) commissures, on the posterior bending (4), and in the inferior branching at the posterior commissure level (5). The cingulum bundle was defined as the grouping of fibres passing through at least a pair of adjacent regions.

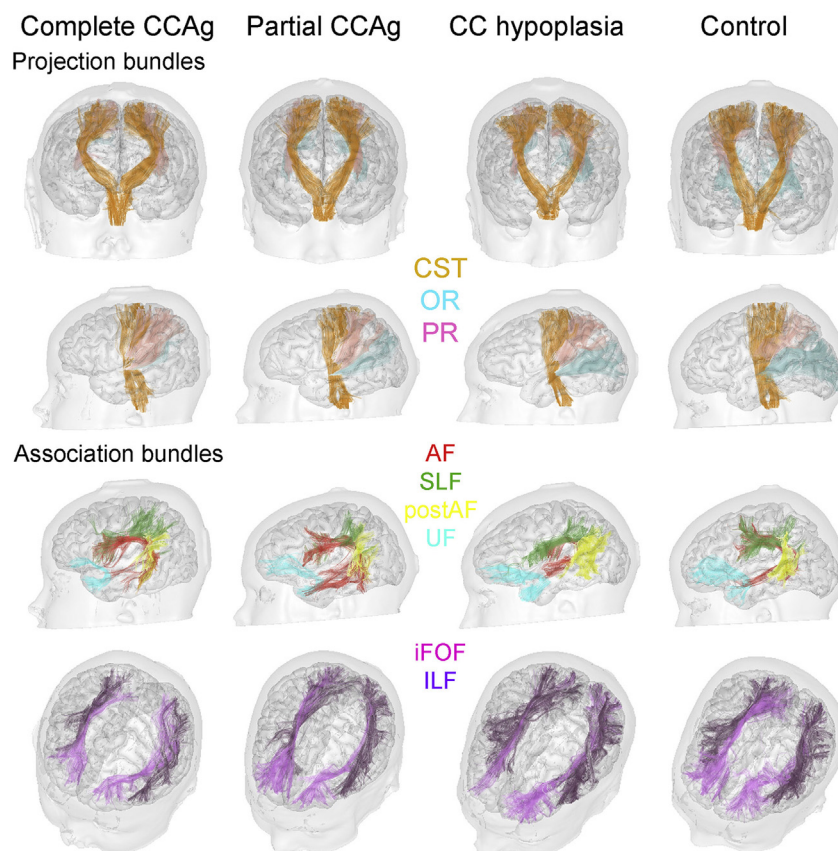


Fig. 4 – Tractography of the main white matter bundles The 3D reconstructions of the white matter bundles obtained on the basis of the adult atlas (Guevara et al., 2012) are presented for the same children as in Fig. 1. Abbreviations: AF: arcuate fasciculus (postAF: posterior segment); CST: corticospinal tract; iFOF: inferior fronto-occipital fasciculus; ILF: inferior longitudinal fasciculus; OR: optic radiations; PR: thalamic radiations projecting to the parietal lobe; SLF: superior longitudinal fasciculus; UF: uncinate fasciculus.

For the Probst bundle, the fibre trajectory was not known a priori, except in its middle portion where it clearly shows a rostrocaudal direction: this portion was small and localised between the anterior and posterior commissures, close to the cingulum. Thus the selection was based on two wide regions drawn at the commissure levels, and cingulum fibres were subtracted to identify Probst fibres. We further eliminated isolated fibres which were not reproducible across subjects by taking advantage of the individual fibre clustering (Guevara et al., 2011): the final Probst tract only included clusters with at least half of the fibres inside the ROI-based tract.

The fornix and the anterior and posterior commissures were not considered in the present study because tracts delineation was adversely affected by partial volume effects with cerebrospinal fluid.

For each bundle, the number of reconstructed virtual fibres was computed. To evaluate the influence of colpocephaly on posterior white matter, we further computed the surface crossed by each posterior bundle on two specific coronal slices (one at the level of anterior vermis, and one posterior to the arcuate fasciculus bending), as well as the surface corresponding to the union of all bundles. Bundles projecting posteriorly were the Probst bundle, the parieto-occipital projections of the corpus callosum, the optic and parietal

radiations, the long and posterior segments of the arcuate fasciculus, the superior and inferior longitudinal fascicles, and the inferior fronto-occipital fasciculus.

2.5. Quantification of DTI parameters

DTI parameters (fractional anisotropy FA, mean diffusivity $\langle D \rangle$) were quantified on average over bundles by taking into account the fibre density (Dubois et al., 2006): medians of DTI parameters were computed while weighting the voxels contributions by the number of fibres passing through. Thus the resulting averages relied more on the bundle core than on partial volume effects with the bundle surrounding. For the bundles selected with the atlas-based approach, the whole reconstructed tracts were considered because of the high reproducibility in tracts morphology among children. In contrast, for the bundles of the “corpus callosum complex”, inter-subject variability in the tract extremities was important. Consequently, only the central segments of each bundle, between the selection regions, were considered for the quantification of DTI parameters (Dubois et al., 2006) (see Figs. 2 and 3a for illustration). Thus, the corpus callosum was segmented around the inter-hemispheric fissure. Above it, the Probst segment was close to the superior segment of the

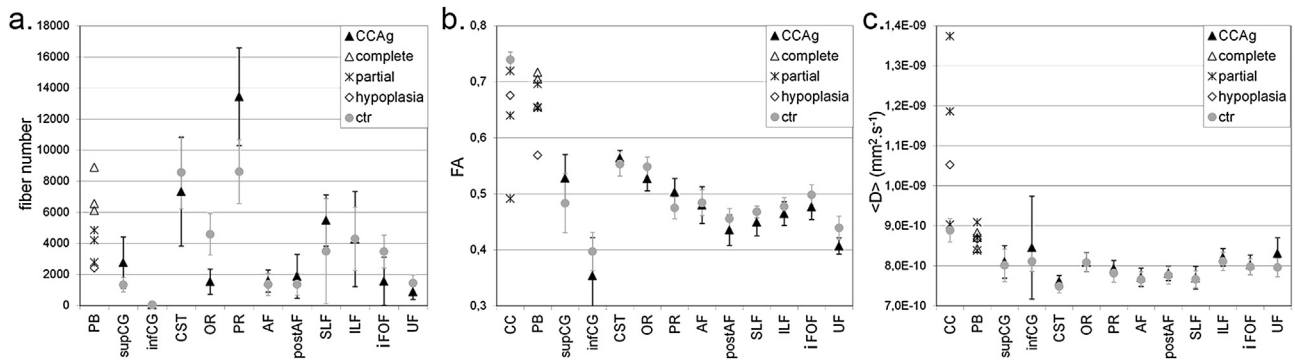


Fig. 5 – Quantification of fibre numbers and DTI parameters within the white matter bundles The numbers of virtual fibres (a), fractional anisotropy (b: FA) and mean diffusivity (c: $\langle D \rangle$) are quantified within the tract segments of the “corpus callosum complex” and within the main white matter bundles. Median values over the dysgenesis and control groups (with standard deviations in error bars) are presented, except for the corpus callosum and the Probst bundles, for which individual values aim to distinguish complete CCAg, partial CCAg and hypoplasia. The number of callosal fibres is not presented because of huge values in control subjects compared with other bundles. Abbreviations: AF: arcuate fasciculus (postAF: posterior segment); CC: corpus callosum; CG cingulum (infCG/supCG: inferior/superior segments); CST: corticospinal tract; iFOF: inferior fronto-occipital fasciculus; ILF: inferior longitudinal fasciculus; OR: optic radiations; PB: Probst bundles; PR: thalamic radiations projecting to the parietal lobe; SLF: superior longitudinal fasciculus; UF: uncinata fasciculus.

cingulum (between the selection regions 2 and 3 as defined in section II.4.), and the cingulum inferior segment was restricted to the temporal lobe (between the selection regions 4 and 5 as defined in section II.4.).

2.6. Quantitative analyses between the dysgenesis and control groups

For each bundle, we evaluated the differences between the children with CCD and the matched controls in terms of the number of reconstructed fibres and DTI parameters, using non-parametric Wilcoxon paired tests. For the corpus callosum, Probst bundle and cingulum, we also looked at differences in fibre number and DTI parameters between the children with complete CCAg, partial CCAg and hypoplasia (mean and standard deviation over each group were computed).

To characterise the microstructure of the Probst bundle, we compared DTI parameters in Probst bundles with those in the controls' corpus callosum on the one hand, and with those in the superior part of dysgenetic cingulum on the other hand (Wilcoxon paired tests). For partial CCAg and hypoplasia, DTI parameters in Probst bundles were also qualitatively compared with DTI parameters in the remnant corpus callosum.

Concerning the bundles reconstructed with the atlas-based approach, we computed asymmetry ratios between the left and right hemispheres $(L - R)/(L + R)$ for fibre numbers and each DTI parameter. When a tract was absent on one side in a given subject, the ratios were set to 0 (and not to -1 or $+1$ as computed conventionally) in order not to bias the asymmetry analyses over the whole group with potential errors in individual tract reconstructions. We first analysed whether asymmetry ratios were different between groups using

Wilcoxon paired tests. Second, we evaluated the presence or absence of asymmetries using Wilcoxon tests within each group independently (if a difference was first observed between the two groups) or within both groups considered together (if no difference was first observed).

The influence of colpocephaly on each posterior bundle was evaluated by comparing the bundle surfaces (on the two coronal slices as defined in section II.4.) among the dysgenesis and control groups using Wilcoxon paired tests. To overcome the bias induced by the slice positions, we only described the results reproducible over the two selected slices. Correlations between each bundle surface and the ventricles surface were further assessed in the dysgenesis group. Equivalent analyses were performed for the surface gather from all posterior bundles.

In all children, the brain size was computed as the sum of left and right hemispheric volumes, which corresponded to the volumes inside the hemispheric hulls (morphological closing of the hemispheric masks) (Germanaud et al., 2012), obtained from T1w images using the Morphologist toolbox (Fischer et al., 2012) of BrainVISA software (<http://brainvisa.info/>).

In all analyses, a statistical threshold of $p < .05$ indicated significance.

3. Results

3.1. Classical description of the dysgenetic brain organisation

The six subjects with corpus callosum agenesis showed the typical features classically described on conventional T1w MRI (Fig. 1): sulci radiating on hemisphere medial surface,

Table 2 – Statistical results. Differences between the dysgenesis and control groups, and inter-hemispheric asymmetries in terms of fibre numbers and DTI parameters, are summarised for each white matter bundle. Statistically significant *p*-values are indicated when Wilcoxon tests were performed.

	Fiber number		FA		<D>	
	Difference between groups	Asymmetry	Difference between groups	Asymmetry	Difference between groups	Asymmetry
CC			trend dysgenetic remnant CC < control CC		dysgenetic remnant CC > control CC	
PB	complete CCAg > partial CCAg > hypoplasia		CCAg > hypoplasia			
supCG	dysgenetic > controls (<i>p</i> = .031)		dysgenetic PB < control CC (<i>p</i> = .016) dysgenetic PB ~ remnant CC dysgenetic PB > supCG (<i>p</i> = .016)		dysgenetic PB < remnant CC dysgenetic PB > supCG (<i>p</i> = .016) related to higher longitudinal diffusivity (<i>p</i> = .016) and lower transverse diffusivity (<i>p</i> = .016)	
CST				difference between groups (<i>p</i> = .016) dysgenetic: right > left (<i>p</i> = .047) controls: no asymmetry		left > right (<i>p</i> = .03)
OR	dysgenetic < controls (<i>p</i> = .016)	left > right (<i>p</i> = .007)	dysgenetic < controls (<i>p</i> = .016)			right > left (<i>p</i> = .045)
PR	dysgenetic > controls (<i>p</i> = .031)					
AF		left > right (<i>p</i> = .043)				
SLF		right > left (<i>p</i> = .011)		right > left (<i>p</i> = .005)		left > right (<i>p</i> = .011)
ILF		left > right (<i>p</i> = .025)				left > right (<i>p</i> = .002)
FOF			dysgenetic < controls (<i>p</i> = .047)			
UF			dysgenetic < controls (<i>p</i> = .016)			

Abbreviations: AF: arcuate fasciculus; CC: corpus callosum; CCAg: agenesis of the corpus callosum; CST: corticospinal tract; <D>: mean diffusivity; FA: fractional anisotropy; ILF: inferior longitudinal fasciculus; OR: optic radiations; PB: Probst bundles; PR: thalamic radiations projecting to the parietal lobe; SLF: superior longitudinal fasciculus; supCG: superior cingulum; UF: uncinata fasciculus.

complete or partial absence of the callosomarginal sulcus and of the cingulate gyrus, reduced white matter volume, enlargement of the posterior part of the lateral ventricles (colpocephaly) and enlargement of the third and fourth ventricles. In the subject with hypoplasia, corpus callosum size was actually reduced on a midsagittal plane but the genu, the body and the splenium seemed to be present (the rostrum was barely detected at the current spatial resolution). Probst bundles were also visualised in both hemispheres of the seven children including in the hypoplasia child (Fig. 1). No child had associated malformation, i.e. all had isolated CCD. Brain size did not differ between the dysgenetic and control groups (mean \pm stddev = 1276 \pm 148 mL, [min, max] = [1025 mL, 1456 mL]). The following quantitative and statistical analyses of fibre numbers and DTI parameters are summarised in Fig. 5 and Table 2.

3.2. Corpus callosum, Probst bundle and cingulum: tractography and DTI results

Corpus callosum fibres were completely absent in three CCAg subjects (Fig. 3a). In three others, they were partially absent, with a callosal connectivity being exclusively frontal in two subjects, and anterior frontal, posterior parietal and occipital in the third one (Fig. 3a). A “sigmoid” bundle was identified in two children with partial CCAg (Fig. 3b): it connected the left frontal region with the right parieto-occipital region through the corpus callosum body in one subject, and the right frontal region with the left parieto-occipital region through the genu in the other subject. In the child with hypoplasia, we found callosal fibres with frontal, parietal, temporal and occipital terminations, but fibres from the body could not be reconstructed due to the thin shape of the remnant corpus callosum compared with the relatively large DTI slice thickness (Fig. 3a).

The comparison of DTI parameters in partial or hypoplastic remnant corpus callosum versus normal corpus callosum revealed higher $\langle D \rangle$ values in the abnormal tracts with a trend towards smaller FA values (Fig. 5, Table 2). It might be explained either by partial volume effects with neighbouring CSF, or by decreased compactness related to the reduced number of fibres.

The Probst bundles were reconstructed by tractography in all CCD subjects, including the subject with hypoplasia (Fig. 3). The tract ran mainly in the rostrocaudal direction, connecting frontal and occipital cortical areas and creating the roof of the lateral ventricles. However, we detected additional fibres that connect parietal and temporal regions. Several fibres also leaved the classical Probst bundle trajectory all along it, and connected cortical regions caudally (Fig. 3a). The anterior Probst fibres blended with the remnant callosal fibres in partial CCAg. As for quantitative analyses, the number of virtual fibres showed a gradient with the degree of dysgenesis (Fig. 5, Table 2). No FA difference was found between the Probst segments of complete and partial CCAg children, but FA was higher in CCAg children than in the child with hypoplasia. $\langle D \rangle$ did not differ between the segments from complete and partial CCAg and hypoplasia children.

The cingulum bundle was reconstructed in all dysgenesis and control children (Fig. 3), despite the absence of cingulate

gyrus in CCAg subjects (Fig. 1). Discrimination between the cingulum and the Probst bundle was coherent between tractography and T1w images, although the two bundles were not easily distinguishable on the DTI-RGB colour-coded directionality map since they both appear with an anterior-posterior direction (green colour). The whole cingulum shape showed no obvious difference between the dysgenesis and control groups. The bundle appeared composed by fibres of different lengths, some leaving the bundle core to connect the grey matter caudally as in Probst bundles (Fig. 3a). The anterior part crossed around the anterior lateral part of the third ventricle's roof in complete CCAg and around the anterior portion of the corpus callosum in other cases. The superior part ran along the outer part of Probst bundle in dysgenesis brains and within the cingulate gyrus in control brains. The posterior part crossed between the posterior lateral part of the third ventricle and the medial part of the lateral ventricles in CCAg, and bended around the splenium of corpus callosum in hypoplasia and controls. In agenetic children, the posterior part followed the Probst bundle beyond cingulum posterior bending, connecting posterior parietal regions. The inferior part dived towards the hippocampus in both groups. In the child with hypoplasia, the cingulum was qualitatively similar to the controls' (Fig. 3a). As for quantitative analyses, the superior segment (close to Probst segment) contained more virtual fibres in dysgenesis children than in controls, but no difference in DTI parameters was found in any segment between groups (Fig. 5, Table 2).

Because the first callosal fibres initially come from the cingulate cortex and because fibres that failed to cross the midline in CCAg brains form the Probst bundle, we further compared DTI parameters across these three bundles (Fig. 5, Table 2). FA values were significantly lower in Probst bundles than in controls' corpus callosum, likely explained by differences in bundles' compactness because $\langle D \rangle$ values were not different. Nevertheless, considering only the four children with partial CCAg and hypoplasia, FA values in Probst bundles were not different from FA values in the callosal remnant fibres, while $\langle D \rangle$ values were lower probably because of partial volume effects with CSF in the corpus callosum. In the dysgenesis group, DTI parameters were significantly different between the Probst bundles and the superior segment of the cingulum despite their close localisation, confirming the different microstructure of these two bundles. All these results together suggest that the Probst bundles present an intermediate compactness and myelination compared with the fibres of the corpus callosum and of the superior cingulum.

3.3. The other bundles: tractography and DTI results

All major white matter bundles defined in the “Guevara atlas” were reconstructed in the same way in both groups (Fig. 4). Their origin, course, ending and global morphology followed the classically described anatomy, and posterior tracts were all found in the patient group despite colpocephaly. Only a few tracts could not be identified with this automatic approach, while retrieved by the conventional approach using manual regions of selection: the right optic radiations in a complete CCAg subject, the right optic radiations and right inferior

fronto-occipital fasciculus in a partial CCAg subject, and the right arcuate fasciculus in a control subject. All bundles were qualitatively not different between the two groups (Fig. 4), with equivalent inter-hemispheric asymmetries in fibre numbers, but some differences were observed in terms of raw fibre numbers and DTI parameters in the patient and control groups, as detailed below and in Fig. 5 and Table 2.

As for projection bundles, the right corticospinal tract of all children showed lower $\langle D \rangle$ than the left one, associated with higher FA in dysgenesis children but no FA asymmetry in control children. The optic radiations showed lower fibre numbers and FA in the dysgenesis group than in the control group, because the colpocephaly either reduced the occipital white matter space or displaced it in comparison with parietal white matter. Actually the atlas-based method may have failed to distinguish the optic and parietal thalamic radiations in the dysgenesis group because the higher number of parietal fibres counterbalanced the reduced number of optic fibres (i.e. no group difference remained when occipital and parietal fibre numbers were summed). In both the dysgenesis and control groups, the optic radiations presented more fibres and lower $\langle D \rangle$ on the left side than on the right side.

As for association bundles, a leftward asymmetry of the arcuate fasciculus was observed in agreement with previous studies of healthy children (Lebel & Beaulieu, 2009): 4 dysgenic brains and 5 control brains actually demonstrated more fibres on the left side, but the 3 other dysgenic brains and 1 control brain were clearly right lateralised. A strong rightward asymmetry was detected in the superior longitudinal fasciculus, with higher fibre number, higher FA and lower $\langle D \rangle$. The inferior longitudinal fasciculus was also asymmetric, with more fibres and higher $\langle D \rangle$ on the left side. Finally, FA in the inferior fronto-occipital and uncinate fascicles was relatively lower in dysgenesis children than in controls.

3.4. Influence of colpocephaly on posterior bundles

All these results together suggest that dysgenic brains present a relatively normal organisation of major white matter bundles, with relatively preserved microstructure and asymmetries. That is why we further investigated whether colpocephaly had an impact on the size of posterior bundles by computing the bundle surfaces on coronal slices. Taking into account only coherent results across the two selected slices, no difference between the dysgenesis and control groups was detected for the total surface resulting from all posterior bundles (including Probst bundle and corpus callosum projections when present), which suggested that colpocephaly had little impact on the overall volume of posterior white matter. No difference was further found for any posterior bundle, except the optic radiations whose surfaces were significantly reduced in the dysgenesis group (anterior slice: $p = .031$; posterior slice: $p = .031$), coherently with the reduced fibre numbers over the whole tract. In this group, a strong negative correlation was further detected between surfaces of the optic radiations and surfaces of the ventricles (correlation coefficients: anterior slice: $R = -.73$; posterior slice $R = -.77$).

4. Discussion

The virtual dissection of major bundles with DWI and tractography enabled us to highlight how CCD impacts brain white matter organisation: only one bundle was missing partly or completely, the corpus callosum; and two bundles were atypical: the Probst bundles in all patients including the one with CC hypoplasia, and the “sigmoid” bundle in two partial CC agenesis. Not only were all posterior bundles present despite colpocephaly, but their macroscopic organisation, microstructure, and their asymmetries were not disturbed in a major way.

4.1. Does Probst bundle gather aberrant callosal fibres?

Two distinct observations supported the hypothesis that Probst bundles were composed by callosal fibres which did not cross the midline: 1) the Probst bundle size was found to depend on the severity of the CCD, and 2) the Probst bundles and the remnant corpus callosum presented relatively similar DTI parameters in dysgenesis children, suggesting close microstructure. Given current knowledge on the embryologic development of the corpus callosum (Ren et al., 2006) and on the failure mechanisms responsible for dysgenesis, axons are supposed to originate from all cortical areas, to head for midline, fail to cross, and end their course in the Probst bundles. Consequently Probst fibres should logically not only be longitudinal, connecting anterior and posterior cortical regions, but rather multidirectional, with projections to lateral regions from the frontal, parietal and temporal lobes. Furthermore, the bundle topography should be spatially organised, in a way similar to the rostrocaudal organisation of the corpus callosum. A previous DTI study has demonstrated that fibres within the Probst bundles are at least partially organised (Utsunomiya, Yamashita, Takano, & Okazaki, 2006): fibres from the frontal pole run more in the bundle's inner side compared with those from a more caudal region of the frontal lobe; fibres from the orbital gyri run along the outermost side of the bundle (Utsunomiya et al., 2006). In contrast, a DTI and immunohistochemical analysis of a mouse model of dysgenesis has shown that Probst ventral fibres exhibited a disorganised structure in comparison with dorsal fibres, and could not be individualised with DTI (Ren, Zhang, Plachez, Mori, & Richards, 2007). In our study, the Probst bundles displayed a frontal, parietal, occipital and temporal pattern of connectivity, with additional fibres reminding the complex connectivity of the corpus callosum to a certain extent. However, these bundles may not have been fully delineated in the present study, since our DWI acquisition protocol and tractography strategy presented some limitations in comparison with HARDI (high angular resolution diffusion imaging) studies (see next section on technical considerations).

Aside from this, the connectivity of the Probst bundles may not only be cortico-cortical, as observed in a knockout mouse model (Alcamo et al., 2008). Wahl and colleagues have further described in a preliminary work using Q-ball imaging that some fibres project into subcortical regions like the thalami and brainstem (Wahl, Barkovich, & Mukherjee, 2010). Actually, axon guidance activity may be disturbed in different

ways depending on the origin of isolated CCAg. This may result in variable and complex patterns of connectivity of the Probst bundle among individuals. These patterns are expected to be more spread than those reported here, and the implementation of dedicated diffusion imaging protocols with high spatial and angular resolution (e.g. HARDI) and the use of probabilistic tractography will probably enable their demonstration in the near future.

In the current study, Probst bundles were interestingly identified in both hemispheres of the CC hypoplasia brain. In a previous study, Tovar-Moll and colleagues also described in a CC hypoplasia brain a thick longitudinal bundle compatible with Probst definition but without apparent separation from the cingulum (Tovar-Moll et al., 2007). In our subject, this bundle was not clearly identifiable on T1w images, but it was clearly distinguishable from cingulum on the colour-coded directionality map (DTI-*RGB*). This distinction was further supported by the different FA values within the two tract segments. We thus hypothesise that for this specific hypoplasia, part of the callosal fibres came from all cortical regions, failed to cross the midline, and subsequently formed a Probst bundle. Actually, different scenarios may result in corpus callosum hypoplasia. In one way, the corpus callosum may be first well developed and an injury or early apoptosis during the foetal period may cause the loss of callosal fibres; this would result in corpus callosum hypoplasia without a Probst bundle. In another way, during callosal fibres migration from all cortical regions, some may cross the midline while others may not, implying the formation of a Probst bundle. Thus DWI may help to refine the large radiological category of hypoplasia into early or late hypoplasia, by detecting or not Probst bundles with tractography.

4.2. What does the remnant corpus callosum connect?

Aside from this, the connectivity pattern of the remnant corpus callosum seems quite complex in brains with partial agenesis. Wahl and colleagues suggested that the process of the development of callosal fragments in partial agenesis is distinct from normal callosal development, and may be influenced by the same signalling mechanisms which yield aberrant intra-hemispheric connectivity through Probst bundles (Wahl et al., 2009). We reconstructed a “sigmoid” bundle in two children with partial CCAg, connecting respectively the right or left frontal region with the contro-lateral parieto-occipital region. Such bundles have been previously described by Tovar-Moll and colleagues, who reported a consistent connection between the right frontal and the left parieto-occipital regions in 4 of 11 patients with partial CCAg (Tovar-Moll et al., 2007). Since these patients had the most severe impairment, they hypothesised that these asymmetric aberrant circuits may relate to the patients' disabilities. However no child in our study had an intellectual disability, and the one with partial CCAg who showed learning difficulties presented an “opposite” sigmoid bundle with connections between the left frontal and the right parieto-occipital regions. The evaluation of more individuals with partial CCAg and further functional investigations with electrophysiology or functional MRI would help to clarify this unclear correlation. Actually, one may also wonder whether this sigmoid bundle could

artefactually result from a mixing between very thin remnant callosal fibres (connecting homotopic regions) and fibres from Probst bundles. Images with higher spatial resolution and smaller slice thickness are required to confirm the possibility of the sigmoid bundle in partial CCAg. Finally, we did not detect any other aberrant bundles in the directionality colour-coded DTI-*RGB* maps of the dysgenetic brains.

4.3. Is the cingulum bundle related to Probst bundle?

Despite the absence of cingulate gyrus (Fig. 1), the cingulum bundle was delineated in all children with CCD, without major shape difference when compared with controls: it is composed of fibres with different lengths, which enables it to increase its connectivity potential (Catani & Thiebaut de Schotten, 2008; Concha, Gross, & Beaulieu, 2005). Contrary to a previous study demonstrating a reduced FA specific to the right cingulum bundle and bilateral reductions in the tract volume (Nakata et al., 2009), we rather observed an increase in the cingulum size (superior segment) in the dysgenesis group compared with the control group, and no difference in DTI parameters.

The Probst bundles were further compared with the cingulum because the cingulate cortex is implied early on in the development of the corpus callosum in the embryo brain: the first callosal axons (known as “pioneering axons”) project homotopically from the cingulate cortex and form the dorsal portion of the developing corpus callosum, while second callosal axons originating from all cortical areas cross the inter-hemispheric midline and form the ventral portion of corpus callosum (Ren et al., 2006). This mechanism may result in the close superior trajectories of the cingulum and Probst bundle in CCAg brains. However we observed with DTI parameters that the two bundles' microstructures differed, suggesting that they are distinct pathways, and validating their delineation and distinction by our tractography methodology.

4.4. Are white matter bundles impaired by CCD?

In our detailed analyses, all major white matter bundles showed similar morphology, organisation (i.e. fibre numbers) and microstructure (i.e. DTI parameters) in dysgenesis and controls brains. Despite these negative results perhaps depending on the low statistical power of our analyses, related to the limited number of subjects, it rather suggests that the absence of callosal fibres does not have a major impact on the establishment of projection and association bundles. We consequently assume that the axonal guidance of these fibres is not impaired, contrary to that responsible for the callosal fibres' guidance through the midline. Colpocephaly was not associated with major variations of posterior bundles, thus it would rather result from missing callosal fibres than from other bundles' anomalies.

4.5. Are white matter asymmetries preserved in the case of CCD?

Furthermore, no difference was detected in terms of inter-hemispheric asymmetries, whereas the development of callosal fibres is supposed to influence anatomical asymmetries.

In particular, the corticospinal tract and the superior longitudinal fasciculus were asymmetric in the same way in CCD and control children.

Functional and anatomical asymmetries have been widely described in the normal brain. The strongest lateralisation relates to language processing, as studied by functional MRI in adults (Herve, Zago, Petit, Mazoyer, & Tzourio-Mazoyer, 2013), infants (Dehaene-Lambertz, Dehaene, & Hertz-Pannier, 2002), and even in preterm newborns as young as 28 weeks of gestational age by functional optical imaging (Mahmoudzadeh et al., 2013). In relation to these functional asymmetries (Dehaene-Lambertz, Hertz-Pannier, & Dubois, 2006), structural asymmetries are already observed in language-related cortical regions (planum temporale, Heschl gyrus, Sylvian fissure, superior temporal sulcus) in the foetal brain (Chi, Dooling, & Gilles, 1977; Dubois, Benders, et al., 2008; Dubois et al., 2010; Glasel et al., 2011; Sowell et al., 2002). The functional lateralisation related to handedness is also linked to anatomical asymmetries in sensory-motor regions (e.g. for the central sulcus) (Sun et al., 2012). As for white matter bundles, strong leftward asymmetry of the arcuate fasciculus is consistently observed in adults (Buchel et al., 2004; Parker et al., 2005; Thiebaut de Schotten, Ffytche, et al., 2011), children (Lebel & Beaulieu, 2009) and infants (Dubois et al., 2009; Liu et al., 2010). The corticospinal tract and the optic radiations also appears left-lateralised (Dubois et al., 2009; Park et al., 2004; Thiebaut de Schotten, Ffytche, et al., 2011), while the inferior fronto-occipital and the superior longitudinal fascicles are right-lateralised (Thiebaut de Schotten, Dell'Acqua, et al., 2011; Thiebaut de Schotten, Ffytche, et al., 2011).

While genetics plays an important role in early hemispheric specialization during embryogenesis, the involvement of the corpus callosum in the establishment of inter-hemispheric asymmetries is discussed (Beaule et al., 2012; Bloom & Hynd, 2005). Exploring patients with CCD should contribute to this debate but results are very limited and controversial to date. Bilateral language representation without clear lateralisation has first been reported during speech production and perception with fMRI (Riecker et al., 2007). However, in a more recent study, no difference in receptive and expressive speech lateralisation was reported between patients and controls, except for frontal regions in the latter task (Pelletier et al., 2011). As for structural asymmetries, strong leftward perisylvian asymmetries for both the planum temporale and planum parietale have been described in a single subject with complete agenesis (Jancke, Staiger, Schlaug, Huang, & Steinmetz, 1997), and asymmetry in white matter microstructure has been investigated only for the ventral cingulum bundle (Nakata et al., 2009) so far.

In the present study of dysgenetic and control children, we found: 1) leftward asymmetries in the arcuate fasciculus in most children (9 out of 14), in the optic radiations and inferior longitudinal fasciculus; and 2) rightward asymmetries in the superior longitudinal fasciculus and corticospinal tract (but only for mean diffusivity). These results confirm previous studies for the arcuate and superior longitudinal fascicles, and the optic radiations. The discrepancy for other bundles may be related either to the different developmental ranges (children versus adults and infants), or to the small size of our groups. Thus further studies in larger cohorts of children with different

ages should clarify this issue. Here our main focus was to evaluate whether dysgenetic and control children show differences in bundles asymmetries, which was not the case.

4.6. Technical considerations

Previous studies of white matter tracts in CCD brains have used deterministic tractography applied to DTI data (Lee et al., 2004; Tovar-Moll et al., 2007) or HARDI data (Forkel et al., 2014; Wahl et al., 2009). Here the bundles' reconstruction was based on an analytical Q-ball model (Descoteaux et al., 2007) and on a tractography algorithm using regularisation (Perrin et al., 2005) in order to deal with crossing fibres, but this approach presented some limitations. Because of acquisition time constraints in children, our DWI protocol included a limited number of diffusion orientations (30) with a relatively low b-value (1000 sec mm⁻²). It only enabled us to compute a 4-order analytical Q-ball model (requiring the estimation of 15 harmonic coefficients), whereas a 6-order model (requiring the estimation of 28 coefficients) is generally used with HARDI data. Reconstructions appeared accurate for most bundles, except in the place of major crossings: in control subjects, the "real shape" of the corpus callosum (with lateral projections) was not correctly reconstructed (see Fig. 3a) in places where callosal fibres cross the corticospinal tract and the corona radiata fibres. Additionally, in CCD children, we may have missed some pathological fibres presenting more crossings than in the normal brain. Using an acquisition protocol with higher radial resolution and b-value and performing global tractography (Fillard, Poupon, & Mangin, 2009) will help to solve this issue in future studies.

To identify white matter bundles from whole brain tractography, automated approaches have recently been proposed to overcome limitations of the region-based approach, which requires a priori knowledge of the bundle anatomical trajectory and localisation. Zhang and colleagues have implemented a DTI-based brain atlas with many three-dimensional regions which can be warped non-linearly to individual DTI datasets to select a large set of long and short bundles (Zhang et al., 2010), but such an approach may fail when dealing with "deformed" brains with CCD since it is based on a normalisation procedure. We used an alternative approach which matched individual datasets with an atlas of fibre bundles according to criteria of distance in the fibre morphology, shape and length (Guevara et al., 2012). One may argue that such a method has not been validated in brains with malformation. Nevertheless this method demonstrated satisfactory and reproducible results over all 14 children in comparison with the selection-region approach (except maybe for the distinction between optic and parietal radiations, as described in the results section). These results are supported by the observation that the major projection and association bundles have equivalent properties in terms of trajectory, shape and length in all CCD and control brains, while their spatial localisation may be shifted by the severe pathological alterations (lack of callosal fibres, presence of Probst bundles and colpocephaly) in CCD brains. Using the Guevara automatic atlas-based approach enabled us to homogenise bundle delineation across children, without requiring both a priori hypothesis on anatomical localisation

and definition of landmarks across subjects for the selection, and to considerably reduce the time needed for data post-processing. This first study may offer a proof of principle for the method utility in clinical practice. Only a few tracts could not be identified with the automatic approach while retrieved by the conventional approach using manual regions of selection. Since the absence of individual tracts on one side was artefactual, the corresponding asymmetry ratios were set to 0 (instead of ± 1), in order not to bias the asymmetry analyses over the whole group.

In our view, the study of the main white matter bundles remains complementary to the evaluation of the global brain network for characterising the cerebral organisation in CCD. Using a connectome framework, Owen and colleagues have recently suggested that structural connectivity in adults with CCAg is much more complex than what can be explained by the simple absence of callosal connectivity (Owen et al., 2013). They reported a reduced global connectivity, an increased local connectivity, a higher inter-individual variability than in controls, and a relatively weak connectivity of the cingulum bundle bilaterally. By contrast, our approach, providing information on individual pathways, suggested no major disturbances of their trajectory and microstructure; particularly the cingulum bundle seemed well preserved. Comparing both approaches in the same CCAg patients thus seems necessary.

4.7. Future directions

Since DTI parameters measured in white matter bundles are supposed to reflect the conduction efficiency of neural responses (Dubois, Dehaene-Lambertz, et al., 2014a; Dubois, Dehaene-Lambertz, et al., 2008), this technique may give indirect information on neuronal activity. Thus our results would suggest that the networks' functioning is relatively similar between the dysgenetic and control groups. Nevertheless considering the aetiology of CCD would be essential to further explore anatomo-functional correlations, because various mechanisms during early fibre development may be impaired by different diseases or disturbances (genetic syndromes, chromosomal abnormalities, metabolic disorders, infections, teratogens, etc.) (Vasudevan et al., 2012). As development outcome is mostly favourable when the dysgenesis is isolated, it can be expected that, in isolated CCD, other inter-hemispheric connections may further supply the lack of callosal fibres: fibres passing through the anterior commissure and indirect connections involving the rhombencephalon and thalamic nuclei should be investigated in future researches. The different functional efficiency of these connections may also explain the inter-individual variability in cognitive performances.

Consequently, structural studies of dysgenetic brain organisation should be complemented with functional imaging evaluations and with patients' behavioural assessment. It would help to understand to what extent disturbed or ectopic white matter pathways impact the cerebral functioning and contributes to the behavioural phenotype, which is highly variable across individuals for still unknown reasons. For instance, Hinkley and colleagues described that abnormal callosal development produces disruptions in the resting-state functional connectivity as measured by

magnetoencephalography (MEG), selectively in the alpha band and in correlation with cognitive impairment (Hinkley et al., 2012). Comparing functional and structural connectivity patterns in the same patients is now the next step to go to highlight the complexity of the developing networks and to explore their underlying mechanisms. As an example, it has recently been suggested that corpus callosum inhibition may actually not be critical for the establishment of lateralised language function (Pelletier et al., 2011): language lateralisation in a receptive speech task was not modified in the case of corpus callosum agenesis, but frontal activations during expressive speech were more bilateral in acallosal participants than in controls. Future anatomo-functional research on younger infants with corpus callosum agenesis will probably open a wide range of opportunities to investigate this question.

5. Conclusion

Detailed anatomical studies of brain organisation are the first step to better understand normal and abnormal cognition. Our study of corpus callosum dysgenetic brains suggests a grossly preserved macro- and microstructure of the main white matter bundles, despite the lack of callosal fibres and the aberrant presence of Probst bundles. Further investigations are required to improve the description of their connectivity patterns and to better understand their implication in cognitive processing and functional lateralisation.

Acknowledgements

The authors thank S. Kulikova for her help with the DWI post-processings, C. Fischer for her help with the Morphologist toolbox, and T. Billette de Villemeur, V. Kieffer and C. Garel for the evaluation of dysgenesis children. A. Bénézit was funded by the "Assistance Publique des Hôpitaux de Paris". This work was supported by the Fyssen Foundation, the McDonnell Foundation, the "Fondation de France", the "Fondation Motrice", the "Ecole des Neurosciences de Paris" and the French National Agency for Research.

REFERENCES

- Aboitiz, F., Scheibel, A. B., Fisher, R. S., & Zaidel, E. (1992). Individual differences in brain asymmetries and fiber composition in the human corpus callosum. *Brain Research*, 598(1–2), 154–161.
- Aboitiz, F., Scheibel, A. B., & Zaidel, E. (1992). Morphometry of the Sylvian fissure and the corpus callosum, with emphasis on sex differences. *Brain*, 115(Pt 5), 1521–1541.
- Alcamo, E. A., Chirivella, L., Dautzenberg, M., Dobрева, G., Farinas, I., Grosschedl, R., et al. (2008). Satb2 regulates callosal projection neuron identity in the developing cerebral cortex. *Neuron*, 57(3), 364–377.
- Beaule, V., Tremblay, S., & Theoret, H. (2012). Interhemispheric control of unilateral movement. *Neural Plasticity*, 2012, 627816.

- Beaulieu, C. (2002). The basis of anisotropic water diffusion in the nervous system – a technical review. *NMR in Biomedicine*, 15(7–8), 435–455.
- Bloom, J. S., & Hynd, G. W. (2005). The role of the corpus callosum in interhemispheric transfer of information: excitation or inhibition? *Neuropsychology Review*, 15(2), 59–71.
- Buchel, C., Raedler, T., Sommer, M., Sach, M., Weiller, C., & Koch, M. A. (2004). White matter asymmetry in the human brain: a diffusion tensor MRI study. *Cerebral Cortex*, 14(9), 945–951.
- Catani, M., Howard, R. J., Pajevic, S., & Jones, D. K. (2002). Virtual in vivo interactive dissection of white matter fasciculi in the human brain. *NeuroImage*, 17(1), 77–94.
- Catani, M., Jones, D. K., & ffytche, D. H. (2005). Perisylvian language networks of the human brain. *Annals of Neurology*, 57(1), 8–16.
- Catani, M., & Thiebaut de Schotten, M. (2008). A diffusion tensor imaging tractography atlas for virtual in vivo dissections. *Cortex*, 44(8), 1105–1132.
- Chadie, A., Radi, S., Trestard, L., Charollais, A., Eurin, D., Verspyck, E., et al. (2008). Neurodevelopmental outcome in prenatally diagnosed isolated agenesis of the corpus callosum. *Acta Paediatrica*, 97(4), 420–424.
- Cherbuin, N., Luders, E., Chou, Y. Y., Thompson, P. M., Toga, A. W., & Anstey, K. J. (2013). Right, left, and center: how does cerebral asymmetry mix with callosal connectivity? *Human Brain Mapping*, 34(7), 1728–1736.
- Chi, J. G., Dooling, E. C., & Gilles, F. H. (1977). Left-right asymmetries of the temporal speech areas of the human fetus. *Archives of Neurology*, 34(6), 346–348.
- Concha, L., Gross, D. W., & Beaulieu, C. (2005). Diffusion tensor tractography of the limbic system. *AJNR (American Journal of Neuroradiology)*, 26(9), 2267–2274.
- Cook, N. D. (1984). Callosal inhibition: the key to the brain code. *Behavioral Science*, 29(2), 98–110.
- Cykowski, M. D., Coulon, O., Kochunov, P. V., Amunts, K., Lancaster, J. L., Laird, A. R., et al. (2008). The central sulcus: an observer-independent characterization of sulcal landmarks and depth asymmetry. *Cerebral Cortex*, 18(9), 1999–2009.
- Dehaene-Lambertz, G., Dehaene, S., & Hertz-Pannier, L. (2002). Functional neuroimaging of speech perception in infants. *Science*, 298(5600), 2013–2015.
- Dehaene-Lambertz, G., Hertz-Pannier, L., & Dubois, J. (2006). Nature and nurture in language acquisition: anatomical and functional brain-imaging studies in infants. *Trends in Neurosciences*, 29(7), 367–373.
- Descoteaux, M., Angelino, E., Fitzgibbons, S., & Deriche, R. (2007). Regularized, fast, and robust analytical Q-ball imaging. *Magnetic Resonance in Medicine*, 58(3), 497–510.
- Dubois, J., Benders, M., Cachia, A., Lazeyras, F., Ha-Vinh Leuchter, R., Sizonenko, S. V., et al. (2008). Mapping the early cortical folding process in the preterm newborn brain. *Cerebral Cortex*, 18(6), 1444–1454.
- Dubois, J., Benders, M., Lazeyras, F., Borradori-Tolsa, C., Leuchter, R. H., Mangin, J. F., et al. (2010). Structural asymmetries of perisylvian regions in the preterm newborn. *NeuroImage*, 52(1), 32–42.
- Dubois, J., Dehaene-Lambertz, G., Kulikova, S., Poupon, C., Hüppi, P. S., & Hertz-Pannier, L. (2014a). The early development of brain white matter: a review of imaging studies in fetuses, newborns and infants. *Neuroscience*, 276(C), 48–71.
- Dubois, J., Dehaene-Lambertz, G., Soares, C., Cointepas, Y., Le Bihan, D., & Hertz-Pannier, L. (2008). Microstructural correlates of infant functional development: example of the visual pathways. *Journal of Neuroscience*, 28(8), 1943–1948.
- Dubois, J., Hertz-Pannier, L., Cachia, A., Mangin, J. F., Le Bihan, D., & Dehaene-Lambertz, G. (2009). Structural asymmetries in the infant language and sensori-motor networks. *Cerebral Cortex*, 19(2), 414–423.
- Dubois, J., Hertz-Pannier, L., Dehaene-Lambertz, G., Cointepas, Y., & Le Bihan, D. (2006). Assessment of the early organization and maturation of infants' cerebral white matter fiber bundles: a feasibility study using quantitative diffusion tensor imaging and tractography. *NeuroImage*, 30(4), 1121–1132.
- Dubois, J., Kulikova, S., Hertz-Pannier, L., Mangin, J. F., Dehaene-Lambertz, G., & Poupon, C. (2014b). Correction strategy for diffusion-weighted images corrupted with motion: application to the DTI evaluation of infants' white matter. *Magnetic Resonance Imaging*, 32(8), 981–992.
- Duclap, D., Schmitt, B., Lebois, A., Riff, O., Guevara, P., Marrakchi-Kacem, L., et al. (2012). Connectomist-2.0: a novel diffusion analysis toolbox for BrainVISA. In *Proceedings of the 29th ESMRMB Meeting* (p. 842).
- Fillard, P., Poupon, C., & Mangin, J. F. (2009). A novel global tractography algorithm based on an adaptive spin glass model. *Medical Image Computing and Computer Assisted Intervention*, 12(Pt 1), 927–934.
- Fischer, C., Operto, G., Laguitton, S., Perrot, M., Denghien, I., Rivière, D., et al. (2012). Morphologist 2012: the new morphological pipeline of BrainVISA. In *Proceedings of the 18th HBM Scientific Meeting, Beijing, China. NeuroImage* (p. 670).
- Forkel, S. J., Thiebaut de Schotten, M., Kawadler, J. M., Dell'acqua, F., Danek, A., & Catani, M. (2014). The anatomy of fronto-occipital connections from early blunt dissections to contemporary tractography. *Cortex*, 56, 73–84.
- Fratelli, N., Papageorghiou, A. T., Prefumo, F., Bakalis, S., Homfray, T., & Thilaganathan, B. (2007). Outcome of prenatally diagnosed agenesis of the corpus callosum. *Prenatal Diagnosis*, 27(6), 512–517.
- Galaburda, A. M. (1984). Anatomical asymmetries. In A. M. Galaburda, & N. Geschwind (Eds.), *Cerebral dominance* (pp. 11–25). Cambridge, MA: Harvard Press.
- Germanaud, D., Lefèvre, J., Toro, R., Fischer, C., Dubois, J., Hertz-Pannier, L., et al. (2012). Larger is twistier: spectral analysis of gyrification (SPANGY) applied to adult brain size polymorphism. *NeuroImage*, 63(3), 1257–1272.
- Glase, H., Leroy, F., Dubois, J., Hertz-Pannier, L., Mangin, J. F., & Dehaene-Lambertz, G. (2011). A robust cerebral asymmetry in the infant brain: the rightward superior temporal sulcus. *NeuroImage*, 58(3), 716–723.
- Glass, H. C., Shaw, G. M., Ma, C., & Sherr, E. H. (2008). Agenesis of the corpus callosum in California 1983–2003: a population-based study. *American Journal of Medical Genetics Part A*, 146A(19), 2495–2500.
- Guevara, P., Duclap, D., Poupon, C., Marrakchi-Kacem, L., Fillard, P., Le Bihan, D., et al. (2012). Automatic fiber bundle segmentation in massive tractography datasets using a multi-subject bundle atlas. *NeuroImage*, 61(4), 1083–1099.
- Guevara, P., Poupon, C., Riviere, D., Cointepas, Y., Descoteaux, M., Thirion, B., et al. (2011). Robust clustering of massive tractography datasets. *NeuroImage*, 54(3), 1975–1993.
- Hellige, J. B. (1993). *Hemispheric asymmetry: What's right and what's left*. Cambridge, MA: Harvard University Press.
- Herve, P. Y., Zago, L., Petit, L., Mazoyer, B., & Tzourio-Mazoyer, N. (2013). Revisiting human hemispheric specialization with neuroimaging. *Trends in Cognitive Sciences*, 17(2), 69–80.
- Hinkley, L. B., Marco, E. J., Findlay, A. M., Honma, S., Jeremy, R. J., Strominger, Z., et al. (2012). The role of corpus callosum development in functional connectivity and cognitive processing. *PLoS One*, 7(8), e39804.
- Huang, H., Zhang, J., van Zijl, P. C., & Mori, S. (2004). Analysis of noise effects on DTI-based tractography using the brute-force

- and multi-ROI approach. *Magnetic Resonance in Medicine*, 52(3), 559–565.
- Isapof, A., Kieffer, V., Sacco, S., Billette de Villemeur, T., Gelot, A., Garel, C., et al. (2010). Impact of prenatal corpus callosum agenesis diagnosis on pregnancy outcome. Evaluation of 155 cases between 2000 and 2006. *Archives de Pédiatrie*, 17(3), 226–232.
- Jancke, L., Staiger, J. F., Schlaug, G., Huang, Y., & Steinmetz, H. (1997). The relationship between corpus callosum size and forebrain volume. *Cerebral Cortex*, 7(1), 48–56.
- Lassonne, M. (1986). The facilitatory influence of the corpus callosum on intrahemispheric processing. In F. Lepore, M. Ptito, & H. H. Jasper (Eds.), *Two hemispheres-one brain: functions of the corpus callosum* (pp. 385–402). New York: Alan Liss.
- Lebel, C., & Beaulieu, C. (2009). Lateralization of the arcuate fasciculus from childhood to adulthood and its relation to cognitive abilities in children. *Human Brain Mapping*, 30(11), 3563–3573.
- Lebel, C., Caverhill-Godkewitsch, S., & Beaulieu, C. (2010). Age-related regional variations of the corpus callosum identified by diffusion tensor tractography. *NeuroImage*, 52(1), 20–31.
- Le Bihan, D., & Johansen-Berg, H. (2012). Diffusion MRI at 25: exploring brain tissue structure and function. *NeuroImage*, 61(2), 324–341.
- Lee, S. K., Mori, S., Kim, D. J., Kim, S. Y., & Kim, D. I. (2004). Diffusion tensor MR imaging visualizes the altered hemispheric fiber connection in callosal dysgenesis. *AJNR (American Journal of Neuroradiology)*, 25(1), 25–28.
- Liu, Y., Baleriaux, D., Kavec, M., Metens, T., Absil, J., Denolin, V., et al. (2010). Structural asymmetries in motor and language networks in a population of healthy preterm neonates at term equivalent age: a diffusion tensor imaging and probabilistic tractography study. *NeuroImage*, 51(2), 783–788.
- Mahmoudzadeh, M., Dehaene-Lambertz, G., Fournier, M., Kongolo, G., Goudjil, S., Dubois, J., et al. (2013). Syllabic discrimination in premature human infants prior to complete formation of cortical layers. *Proceedings of the National Academy of Sciences of the United States of America*, 110(12), 4846–4851.
- Moutard, M. L., Kieffer, V., Feingold, J., Lewin, F., Baron, J. M., Adamsbaum, C., et al. (2012). Isolated corpus callosum agenesis: a ten-year follow-up after prenatal diagnosis (how are the children without corpus callosum at 10 years of age?). *Prenatal Diagnosis*, 32(3), 277–283.
- Nakata, Y., Barkovich, A. J., Wahl, M., Strominger, Z., Jeremy, R. J., Wakahiro, M., et al. (2009). Diffusion abnormalities and reduced volume of the ventral cingulum bundle in agenesis of the corpus callosum: a 3T imaging study. *AJNR (American Journal of Neuroradiology)*, 30(6), 1142–1148.
- Owen, J. P., Li, Y. O., Ziv, E., Strominger, Z., Gold, J., Bukhpun, P., et al. (2013). The structural connectome of the human brain in agenesis of the corpus callosum. *NeuroImage*, 70, 340–355.
- Park, H. J., Westin, C. F., Kubicki, M., Maier, S. E., Niznikiewicz, M., Baer, A., et al. (2004). White matter hemisphere asymmetries in healthy subjects and in schizophrenia: a diffusion tensor MRI study. *NeuroImage*, 23(1), 213–223.
- Parker, G. J., Luzzi, S., Alexander, D. C., Wheeler-Kingshott, C. A., Ciccarelli, O., & Lambon Ralph, M. A. (2005). Lateralization of ventral and dorsal auditory-language pathways in the human brain. *NeuroImage*, 24(3), 656–666.
- Paul, L. K., Brown, W. S., Adolphs, R., Tyszka, J. M., Richards, L. J., Mukherjee, P., et al. (2007). Agenesis of the corpus callosum: genetic, developmental and functional aspects of connectivity. *Nature Reviews Neuroscience*, 8(4), 287–299.
- Pelletier, I., Paquette, N., Lepore, F., Rouleau, I., Sauerwein, C. H., Rosa, C., et al. (2011). Language lateralization in individuals with callosal agenesis: an fMRI study. *Neuropsychologia*, 49(7), 1987–1995.
- Perrin, M., Poupon, C., Cointepas, Y., Rieul, B., Golestani, N., Pallier, C., et al. (2005). Fiber tracking in q-ball fields using regularized particle trajectories. *Information Processing Medical Imaging*, 19, 52–63.
- Probst, M. (1901). Ueber den Bau des vollständigen balkenlosen Grobhirns. *Archives of Psychiatric Nursing*, 34, 709–786.
- Ren, T., Anderson, A., Shen, W. B., Huang, H., Plachez, C., Zhang, J., et al. (2006). Imaging, anatomical, and molecular analysis of callosal formation in the developing human fetal brain. *Anatomical Record. Part A, Discoveries in Molecular, Cellular, and Evolutionary Biology*, 288(2), 191–204.
- Ren, T., Zhang, J., Plachez, C., Mori, S., & Richards, L. J. (2007). Diffusion tensor magnetic resonance imaging and tract-tracing analysis of Probst bundle structure in Netrin1- and DCC-deficient mice. *Journal of Neuroscience*, 27(39), 10345–10349.
- Riecker, A., Ackermann, H., Schmitz, B., Kassubek, J., Herrnberger, B., & Steinbrink, C. (2007). Bilateral language function in callosal agenesis: an fMRI and DTI study. *Journal of Neurology*, 254(4), 528–530.
- Riviere, D., Papadopoulos-Orfanos, D., Poupon, C., Poupon, F., Coulon, O., Poline, J. B., et al. (2000). A structural browser for human brain mapping. In , 11. *Proceedings of the 6th HBM Scientific Meeting, San Antonio, USA. NeuroImage* (p. S912).
- Sowell, E. R., Thompson, P. M., Rex, D., Kornsand, D., Tessner, K. D., Jernigan, T. L., et al. (2002). Mapping sulcal pattern asymmetry and local cortical surface gray matter distribution in vivo: maturation in perisylvian cortices. *Cerebral Cortex*, 12(1), 17–26.
- Sun, Z. Y., Kloppel, S., Riviere, D., Perrot, M., Frackowiak, R., Siebner, H., et al. (2012). The effect of handedness on the shape of the central sulcus. *NeuroImage*, 60(1), 332–339.
- Takao, H., Abe, O., Yamasue, H., Aoki, S., Sasaki, H., Kasai, K., et al. (2011). Gray and white matter asymmetries in healthy individuals aged 21–29 years: a voxel-based morphometry and diffusion tensor imaging study. *Human Brain Mapping*, 32(10), 1762–1773.
- Takao, H., Hayashi, N., & Ohtomo, K. (2011). White matter asymmetry in healthy individuals: a diffusion tensor imaging study using tract-based spatial statistics. *Neuroscience*, 193, 291–299.
- Thiebaut de Schotten, M., Dell'Acqua, F., Forkel, S. J., Simmons, A., Vergani, F., Murphy, D. G., et al. (2011). A lateralized brain network for visuospatial attention. *Nature Neuroscience*, 14(10), 1245–1246.
- Thiebaut de Schotten, M., Ffytche, D. H., Bizzi, A., Dell'Acqua, F., Allin, M., Walshe, M., et al. (2011). Atlasing location, asymmetry and inter-subject variability of white matter tracts in the human brain with MR diffusion tractography. *NeuroImage*, 54(1), 49–59.
- Tovar-Moll, F., Moll, J., de Oliveira-Souza, R., Bramati, I., Andreiuolo, P. A., & Lent, R. (2007). Neuroplasticity in human callosal dysgenesis: a diffusion tensor imaging study. *Cerebral Cortex*, 17(3), 531–541.
- Utsunomiya, H., Yamashita, S., Takano, K., & Okazaki, M. (2006). Arrangement of fiber tracts forming Probst bundle in complete callosal agenesis: report of two cases with an evaluation by diffusion tensor tractography. *Acta Radiologica*, 47(10), 1063–1066.
- Vasudevan, C., McKechnie, L., & Levene, M. (2012). Long-term outcome of antenatally diagnosed agenesis of corpus callosum and cerebellar malformations. *Seminars in Fetal & Neonatal Medicine*, 17(5), 295–300.
- Wahl, M., Barkovich, A. J., & Mukherjee, P. (2010). Diffusion imaging and tractography of congenital brain malformations. *Pediatric Radiology*, 40(1), 59–67.
- Wahl, M., Strominger, Z., Jeremy, R. J., Barkovich, A. J., Wakahiro, M., Sherr, E. H., et al. (2009). Variability of

- homotopic and heterotopic callosal connectivity in partial agenesis of the corpus callosum: a 3T diffusion tensor imaging and Q-ball tractography study. *AJNR (American Journal of Neuroradiology)*, 30(2), 282–289.
- Witelson, S. F. (1989). Hand and sex differences in the isthmus and genu of the human corpus callosum. A postmortem morphological study. *Brain*, 112(Pt 3), 799–835.
- Witelson, S. F., & Nowakowski, R. S. (1991). Left out axons make men right: a hypothesis for the origin of handedness and functional asymmetry. *Neuropsychologia*, 29(4), 327–333.
- Zhang, Y., Zhang, J., Oishi, K., Faria, A. V., Jiang, H., Li, X., et al. (2010). Atlas-guided tract reconstruction for automated and comprehensive examination of the white matter anatomy. *NeuroImage*, 52(4), 1289–1301.